Talanta 267 (2024) 125155

Contents lists available at ScienceDirect

Talanta

journal homepage: www.elsevier.com/locate/talanta

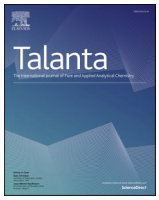

Disposable electrochemical immunoplatform to shed light on the role of the multifunctional glycoprotein TIM-1 in cancer cells invasion

Jennifer Quinchia [a,b,1], Marina Blázquez-García [a,1], Rebeca M. Torrente-Rodríguez [a], Víctor Ruiz-Valdepeñas Montiel [a], Verónica Serafín [a], Raquel Rejas-González [c], Ana Montero-Calle [c], Jahir Orozco [b], José M. Pingarrón [a], Rodrigo Barderas [c,*], Susana Campuzano [a,**]

[a] Department of Analytical Chemistry, Faculty of Chemistry, Complutense University of Madrid, Pza. de Las Ciencias 2, 28040, Madrid, Spain
[b] Max Planck Tandem Group in Nanobioengineering, Institute of Chemistry, Faculty of Natural and Exact Sciences, University of Antioquia. Complejo Ruta N, Calle 67 No. 52-20, Medellín, 050010, Colombia
[c] UFIEC, Instituto de Salud Carlos III, 28220, Majadahonda, Madrid, Spain

ARTICLE INFO

Handling Editor: Agata Michalska

Keywords:
TIM-1
Amperometric detection
Immunoplatform
Screen-printed carbon electrode
Magnetic particles
Breast and lung cancer

ABSTRACT

Detecting overexpression of cancer biomarkers is an excellent tool for diagnostic/prognostic and follow-up of patients with cancer or their response to treatment. This work illustrates the relevance of interrogating the levels of T-cell immunoglobulin and mucin domain 1 (TIM-1) protein as a diagnostic/prognostic biomarker of high-prevalence breast and lung cancers by using an amperometric disposable magnetic microparticles-assisted immunoplatform. The developed method integrates the inherent advantages of carboxylic acid-functionalized magnetic beads (HOOC-MBs) as pre-concentrator support and the amperometric transduction at screen-printed carbon electrodes (SPCEs). The immunoplatform involves a sandwich-type immunoassay assembled on HOOC-MBs through the specific capture/labeling of TIM-1 using capture antibodies and horseradish peroxidase (HRP)-conjugated biotinylated detection antibodies as biorecognition elements. The magnetic immunoconjugates were confined onto the working electrode (WE) surface of the SPCEs for amperometric detection using the hydroquinone/hydrogen peroxide/HRP (HQ/H_2O_2/HRP) redox system. The method allows the selective detection of TIM-1 protein over the 87–7500 pg mL^{-1} concentration range in only 45 min, with a limit of detection of 26 pg mL^{-1}. The developed bioplatform was successfully applied to the analysis of breast and lung cancer cell extracts, providing the first quantitative results of the target glycoprotein in these types of samples.

1. Introduction

T-cell immunoglobulin and mucin domain 1 (TIM-1), also called hepatitis A cellular receptor 1 (HAVcR1), and kidney injury molecule 1 (KIM-1), is a mucin-like class I integral membrane glycoprotein. TIM-1 encodes a 359-amino acids membrane protein containing a putative signal sequence (residues 1–20), an N-terminal cysteine (Cys)-rich immunoglobulin G-like (IgG-) domain, a mucin-like domain (residues 130–205), a transmembrane domain (residues 291–311), and a 50-amino acid long cytoplasmic tail that contains tyrosine phosphorylation motifs involved in transmembrane signaling [1,2]. TIM-1 has multiple functions associated with susceptibility to kidney injury [3–5], atopic (e.g., asthma and allergy) and autoimmune diseases (e.g., rheumatoid arthritis) [6–8], infections (e.g., caused by hepatitis C virus, human immunodeficiency (HIV) virus, hepatitis A virus, and *Helicobacter pylori* bacterium) [1,9–11], and cancer (e.g., bladder, cholangio, head and neck, colorectal, gastric, kidney, liver, lung adenocarcinoma, breast, skin, uterine corpus endometrial, and pancreatic) [12–16].

TIM-1 is a critical protein in cancer biology due to its heterogeneity, but few studies address the role of TIM-1 in tumorigenesis. Some authors reported that TIM-1 has a function in regulating tight junctions (TJs) of

* Corresponding author.
** Corresponding author.
E-mail addresses: r.barderasm@isciii.es (R. Barderas), susanacr@quim.ucm.es (S. Campuzano).
[1] The authors contributed equally.

https://doi.org/10.1016/j.talanta.2023.125155
Received 31 July 2023; Received in revised form 24 August 2023; Accepted 2 September 2023
Available online 4 September 2023

human endothelial cells [17] and that overexpression of TIM-1 causes the TJ structures to lose cohesiveness, making cancer cells invasive and ultimately resulting in metastasis [12]. TIM-1 has also been reported to block cell differentiation and its overexpression to increase the incidence of infection and promote susceptibility to cancer [12]. More recently, TIM-1 has been showed to be cleaved proximal to the plasma membrane, releasing the TIM-1 ectodomain, which may have importance in angiogenesis via the activation of the interleukin 6/signal transducer and activation of the transcription 3/hypoxia-inducible factor 1-alpha (IL-6/STAT3/HIF-1α) pathway [13]. Therefore, TIM-1 emerges as a promising cancer biomarker associated with susceptibility, tumor growth, and progression [12,14,16]. Moreover, in those cancers where the TIM-1 ectodomain is not shed in the urine, it may be in circulation, enabling TIM-1 to be a biomarker for the non-invasive diagnosis of multiple cancers. Remarkably, studies have indicated that the overexpression of TIM-1 is associated with a low overall survival (OS) rate in non-small-cell lung carcinoma (NSCLC) [14] as well as the TIM-1 clinical relevance for predicting invasive breast cancers [18]. Therefore, the TIM-1 diagnostic and prognostic value in these types of cancers make its detection imperative.

Different methods have been reported for detecting TIM-1 related to kidney injury and as a urine biomarker. These include high electron mobility transistor (HEMT) [19], enzyme-linked immunosorbent (ELISA) [20], immunochromatographic lateral flow [19], microsphere-based Luminex xMAP- [21], miniaturized nuclear magnetic resonance [22], and optical [23–25], photoelectrochemical [26], and electrochemical [27–30] biosensors. Among them, electrochemical biosensors are attractive due to their high sensitivity, selectivity, affordability, simplicity in manufacturing and handling, and real-time response. More importantly, these biosensors can be miniaturized and integrated within multiplexed formats to simultaneously detect multiple tumor biomarkers in different clinical ranges or/and at different molecular levels as point-of-care testing (POCT) solutions [31–33]. Indeed, electrochemical biosensors have been widely exploited for the determination of cancer-related biomarkers, including breast and lung cancer [34–36], since they can exploit all the advantages of electrochemical methods, biosensing and nano or micromaterials/structures to improve the sensitivity and specificity of the resulting devices [37–39]. For example, magnetic particles (MBs) have been widely employed in recent years in electrochemical biosensing. As a multifunctional material, MBs overcome diffusion limitations during the biorecognition element-target affinity binding, enable simple and efficient sample cleanup and preconcentration by an external magnetic field, and avoid non-specific adsorptions. In addition, MBs enhance the analytical performance of electrochemical biosensing for the detection of targets of different nature within a wide range of complex matrices [40–43] and show good storage stability after simple and reproducible modification, which maximizes their potential for implementation in POCT devices.

Assuming all that mentioned above, this work takes advantage of the unique properties of MBs for the development of an electrochemical immunoplatform, competitive in terms of simplicity, short preparation time, and applicability to complex samples, in comparison with other biosensing strategies reported in the literature [26–30], which needed the use of nanomaterials, required multiple steps, involved lengthy preparation times, and were only applied to supplemented biological samples.

2. Materials and methods

2.1. Reagents and solutions

Carboxylic acid-functionalized magnetic beads (HOOC-MBs, 2.8 μm Ø, 2×10^9 particles mL^{-1}, Dynabeads™ M − 270 carboxylic acid, Cat. No.: 14305D), commercial blocker™ casein solution (BB, PBS pH 7.4 containing 1.0% w/v purified casein, Cat. No.: 37,528), and 1-(3-dimethylaminopropyl)-3-ethylcarbodiimide hydrochloride (EDC-HCl) were purchased from Thermo Fisher Scientific (Waltham, Massachusetts, United States). *N*-hydroxysulfosuccinimide sodium salt (sulfo-NHS, 99.0%) was purchased from Fluorochem (Hadfield, Derbyshire, United Kingdom). 2-(*N*-morpholino)ethanesulfonic acid (MES, ≥99.0%) was purchased from GERBU Biotechnik GmbH (Heidelberg, Baden-Württemberg, Germany). Potassium chloride (KCl, ≥99.0%), disodium hydrogen phosphate (Na_2HPO_4), sodium chloride (NaCl, ≥99.0%), sodium dihydrogen phosphate dihydrate ($NaH_2PO_4{\cdot}2H_2O$), and tris (hydroxymethyl)aminomethane hydrochloride (Tris-HCl, ≥99.0%) were purchased from Scharlab (Sentmenat, Barcelona, Spain). Ethanolamine (ETA, ≥98.0%), hydrogen peroxide (H_2O_2, 30% w/w in H_2O), hydroquinone (HQ, 99.0%), and streptavidin-horseradish peroxidase conjugate (Strep-HRP, 500 U mL^{-1}, Ref.: 11,089,153,001 from Roche) were purchased from Sigma-Aldrich (Saint Louis, Missouri, United States).

Recombinant human TIM-1 standard, mouse anti-human TIM-1 capture antibody (CAb), and biotinylated goat anti-human TIM-1 detection antibody (b-DAb) as the components of the human TIM-1/KIM-1/HAVCR DuoSet ELISA (Cat. No.: DY972) were purchased from R&D Systems (Minneapolis, Minnesota, United States).

Potential interfering non-target proteins tested in the selectivity studies include human hemoglobin (Hb, Ref.: H7379), human serum albumin (HSA, ≥96%, Ref.: A1653), and human serum immunoglobulin G (IgG, ≥95%, Ref.: I2511) purchased from Sigma-Aldrich (Saint Louis, Missouri, United States); recombinant human tumor necrosis factor-alpha protein (TNF-α, ≥96%, Cat. No.: 554,618) purchased from BD Bioscience (Franklin Lakes, New Jersey, United States); recombinant human interleukin-13 receptor alpha-2 (IL-13Rα2, from Human IL-13Rα2 DuoSet ELISA, Cat. No.: DY614), and recombinant human periostin protein (POSTN, from Human Periostin/OSF-2 DuoSet ELISA, Cat. No.: DY3548B) purchased from R&D Systems (Minneapolis, Minnesota, United States).

All chemicals were used without further purification unless otherwise stated. Bioreagents were prepared according to the corresponding reagent preparation procedures. The following buffer solutions were used: 0.025 M MES, pH 5.0; 1X phosphate-buffered saline (PBS) containing 0.01 M phosphate, 0.137 M NaCl, and 0.0027 M KCl, pH 7.5; 5X phosphate-buffered (PB) containing 0.05 M phosphate, pH 6.0; 10X PB containing 0.1 M phosphate, pH 8.0; 0.1 M Tris-HCl, pH 7.2. Deionized water type I from a Millipore Milli-Q purification system (18.2 MΩ cm) was used for the preparation of all buffer solutions.

Other solutions include EDC-HCl/Sulfo-NHS mixture solution (50 mg mL^{-1} each) prepared in 0.025 M MES, pH 5.0, and 1.0 M ETA solution prepared in 10X PB, pH 8.0 for HOOC-MBs activation and blocking steps, respectively. For electrochemical measurements, 0.1 M HQ and 0.1 M H_2O_2 stock solutions were prepared in 5X PB, pH 6.0 before use.

2.2. Instruments and techniques

Amperometric measurements were performed with a CHI812B model potentiostat (CH Instruments, Austin, Texas) with the CHI812B software. Screen-printed electrodes (SPEs) were connected to the potentiostat through a cable connector for SPEs (Ref.: DRP-CAC); both were purchased from Metrohm DropSens (Asturias Technology Park, Spain). Screen-printed carbon electrodes (SPCEs, Ref.: DRP-110) consisting of a three-electrode cell configuration with a 4 mm working electrode (WE), a carbon counter electrode (CE), and a silver (Ag) pseudo-reference electrode, all printed on a ceramic substrate, were used.

Homogenization of the solutions was facilitated by a Wizard IR Vortex (VELP Scientifica, Usmate-velate, Lombardy, Italy). A MS-100 thermoshaker incubator (Universal Labortechnik GmbH, Leipzig, Saxony, Germany) was used for MBs modification. Magnetic separation after modification/washing steps was made using a magnetic particles' concentrator (DynaMag™-2, Cat. No.: 12321D, Thermo Fisher

Scientific, Waltham, Massachusetts, United States). A homemade polymethylmethacrylate (PMMA) holding casing with an embedded neodymium magnet (AIMAN GZ, Meco, Madrid, Spain) was used to ensure reproducible, stable, and uniform confinement of the resultant magnetic immunoconjugates onto the WE surface of the SPCEs before performing amperometric detection.

2.3. Experimental procedures

2.3.1. Assembly of HRP-labeled sandwich-type magnetic immunoconjugates

The whole protocol was carried out in 1.5 mL microcentrifuge tubes. The sequential modification steps were performed with 25 μL of the corresponding solution in a thermoshaker at 25 °C under continuous stirring (950 rpm). All washing steps were performed with a volume of 50 μL. After each modification/washing step, the microcentrifuge tubes containing the magnetic conjugates suspensions were placed in the magnetic particles' concentrator for 2 min before removing the supernatant without losing MBs.

The optimized procedure for the modification of HOOC-MBs was carried out as follows. A 3 μL-aliquot of the HOOC-MBs suspension was placed in a 1.5 mL microcentrifuge tube and washed twice with 0.025 M MES, pH 5.0 for 10 min under the conditions stated above. Next, the washed HOOC-MBs were resuspended in 25 μL of freshly prepared EDC-HCl/Sulfo-NHS mixture solution and incubated for 35 min to activate the carboxylic acid groups, followed by two washing steps with 0.025 M MES, pH 5.0. Next, covalent immobilization of CAb was performed by resuspending activated HOOC-MBs in 25 μL of a 50 μg mL^{-1} CAb solution prepared in 0.025 M MES, pH 5.0, and incubating for 15 min. After two washing steps with the same buffered media, the remaining activated groups were blocked by incubation with 25 μL of a 1.0 M ETA solution for 60 min. Subsequently, the blocked CAb/MBs were washed once with 0.1 M Tris-HCl, pH 7.2 and twice with BB. Binding of the TIM-1 protein involved resuspension of blocked CAb/MBs in 25 μL of a solution containing TIM-1 standard protein prepared in BB and incubation for 15 min, followed by two washing steps with BB. The HRP-labeled sandwich-complexes were formed by incubating TIM-1/CAb/MBs with 25 μL of 1.0 μg mL^{-1} b-DAb and 1/500 diluted Strep-HRP mixture solution prepared in BB for 30 min, followed by two final washing steps with BB.

Before the amperometric readout, the Strep-HRP/b-DAb/TIM-1/CAb/MBs were resuspended in 50 μL of 5X PB pH 6.0.

2.3.2. Amperometric readout

The resuspended Strep-HRP/b-DAb/TIM-1/CAb/MBs were confined onto the WE surface of the SPCEs previously placed in the neodymium magnet-encapsulated holding casing. Then, the assembled Strep-HRP/b-DAb/TIM-1/CAb/MBs/SPCE/magnetic holding casing was immersed into a 10 mL glass electrochemical cell containing 10 mL of 1.0 mM HQ solution prepared in 5X PB pH 6.0. Amperometric readouts started to be recorded in stirred solutions by applying a reduction potential of −0.20 V (*vs.* Ag pseudo-reference electrode). 50 μL of 0.1 M H_2O_2 were added when the background current was stabilized, and the amperometric measurement was continued until the steady-state was reached again. The cathodic amperometric responses (-i, in nA) given through the text correspond to the difference between the background and steady-state currents before and after H_2O_2 addition, respectively.

2.3.3. Analysis of biological samples

The analyzed samples were lysates of breast (MDA-MB-231, MCF7, and SkBr3) and lung (A549) cancer cultured cells obtained from the American Type Culture Collection (ATCC) cell repository. The cells were grown at confluency and the protein extracts obtained as previously described [44] and stored at −80 °C until use. The concentration of the extracts was determined in μg μL^{-1} using the tryptophan method [45] and the desired protein amount was analyzed by diluting the appropriate volume in the corresponding buffer. Cell extracts were also semi-quantitatively analyzed by Western blot (WB). To do this, 10 μg of each cell extract were used and probed with b-DAb followed by its corresponding HRP-labeled secondary antibody. TIM-1 specific chemiluminescence signals were developed using the electrochemiluminescence (ECL) Western blotting substrate (Thermo Fisher Scientific, Waltham, MA, USA) [46]. Signals were recorded on an Amersham Imager 680 (GE Healthcare, Chicago, IL, USA). Protein band intensities were quantified using ImageJ Software and normalized using GAPDH as loading control.

2.3.4. Statistical analysis

All experiments were performed in triplicate, and the results were presented as the mean value ± standard deviation ($\bar{x} \pm s$). One-way analysis of variance (ANOVA) with Tukey's post hoc test was performed to evaluate the statistically significant differences between more than two interfering non-target proteins with a level of statistical significance of 95% ($\alpha = 0.05$). A control chart was constructed using the signal-to-blank ratio (S/B) for stability studies by taking the average of three measurements as the central value ($\bar{x}_{S/B}$) and three times its standard deviation ($\bar{x}_{S/B} \pm 3s_{S/B}$) as the upper and lower control limits, respectively. Student's t-test was used to study the matrix effect in the analysis of cell extracts.

3. Results and discussion

The sequential steps for assembling the HRP-labeled sandwich-type immunocomplexes on MBs as well as the fundamentals of the amperometric readout for the detection of TIM-1 are schematized in Fig. 1. The developed immunoplatform implied the sequential modification of HOOC-MBs, first by immobilizing CAbs through covalent EDC-HCl/Sulfo-NHS chemistry, to specifically capture the TIM-1 protein, further sandwiched with b-DAbs labeled with Strep-HRP conjugates. Subsequently, the Strep-HRP/b-DAb/TIM-1/CAb/MBs were confined on the WE surface of the SPCE, which was previously placed on a magnetic holding casing, and then introduced into the electrochemical cell. The biorecognition events were monitored by amperometry using the HQ/H_2O_2/HRP redox system, where HQ worked as an efficient electron transfer mediator to transport electrons from the HRP's catalytic center to the WE surface. $HRP_{(RED)}$ in the presence of H_2O_2 catalyzes the oxidation of HQ to benzoquinone (BQ), which is reduced back at the electrode surface by applying a −0.20 V constant potential (*vs.* the Ag pseudo-reference electrode) [47,48]. According to the assay setup, the

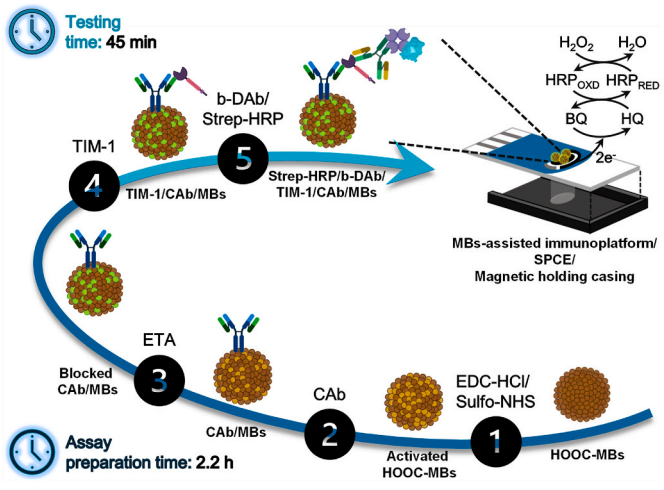

Fig. 1. Scheme displaying the assembly of Strep-HRP/b-DAb/TIM-1/CAb/MBs and the reactions involved in the amperometric transduction at SPCEs using the HQ/H_2O_2/HRP redox system.

resulting cathodic currents are directly proportional to the TIM-1 concentration in the sample.

3.1. Optimization of critical experimental variables involved in the determination of TIM-1

The key experimental variables affecting the analytical performance of the electrochemical immunoplatforms were evaluated using univariate analysis. The amperometric responses obtained in the presence of 2500 pg mL^{-1} (signal, S) and the absence (blank, B) of TIM-1 were compared for each value of the tested range. The values providing better discrimination between such amperometric responses (i.e., higher S/B ratios) were selected for further experiments. The selected values neither compromised simplicity, cost affordability, reproducibility, nor assay time.

The starting protocol for the optimizations involved four steps with (i) 25 μg mL^{-1} CAb, (ii) 0 and 2500 pg mL^{-1} TIM-1 standard protein, (iii) 1.0 μg mL^{-1} b-DAb, and (iv) 1/1000 diluted Strep-HRP solutions. Each step lasted for 30 min. The amount of HOOC-MBs, and their activation and blocking steps were kept constant according to that described in Section 2.3.1. All the concentrations of the bioreagents, incubation times, and assembly protocol were investigated experimentally. All other relevant variables, including the amount of HOOC-MBs, and the variables affecting the amperometric readout, were previously optimized [49,50]. Moreover, the working conditions used in the HOOC-MBs activation procedure, the blocking step of the remaining activated carboxylic groups, and the successive washings were made according to the protocol provided by the MBs supplier. Fig. 2 shows the dependence of the amperometric responses in the presence of 2500 pg mL^{-1}, the absence of TIM-1 standard protein, and the resulting S/B ratio

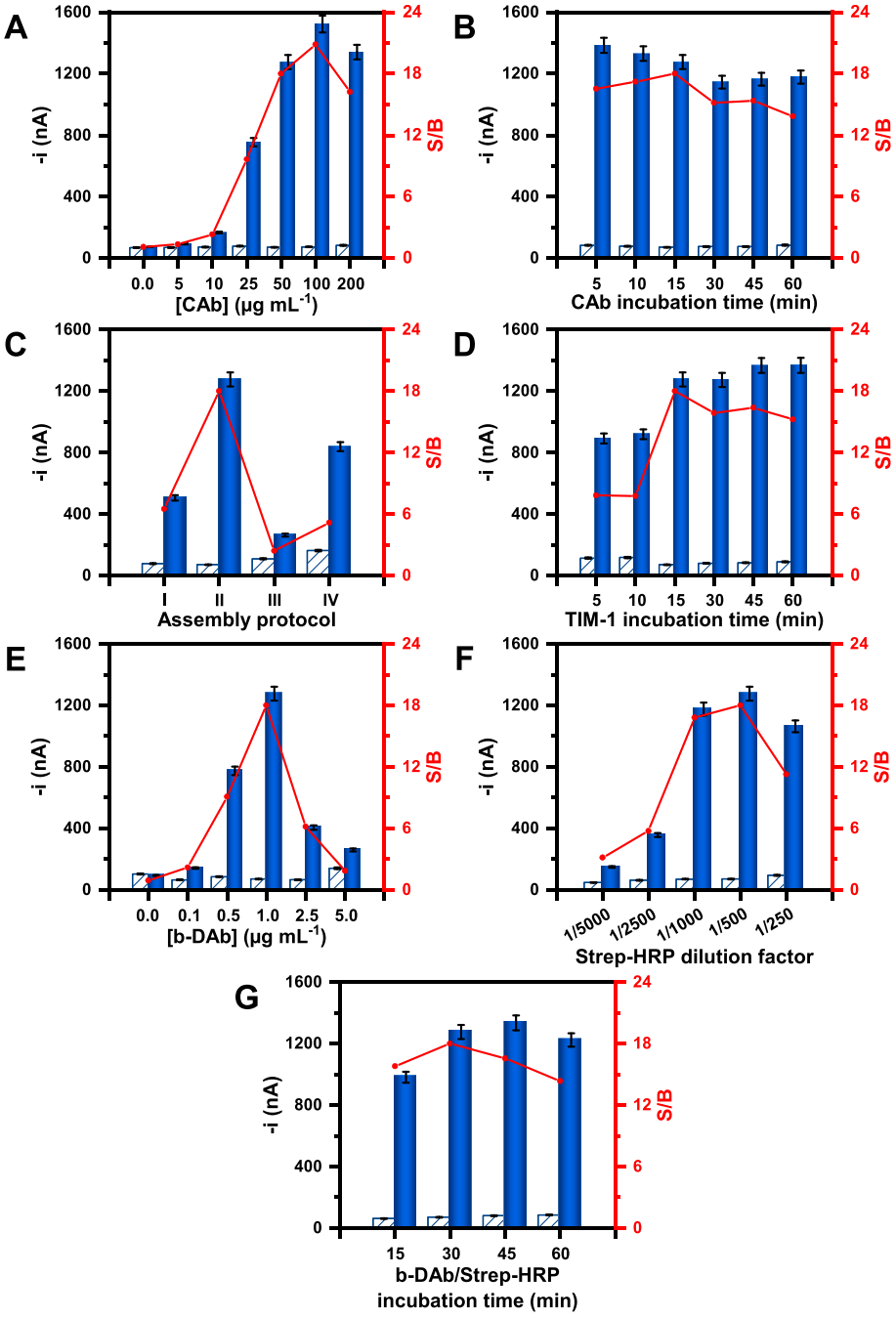

Fig. 2. Dependence of the amperometric responses measured in the presence of 2500 pg mL^{-1} (blue bars, S) and absence (white pattern bars, B) of TIM-1 standard protein and the resulting signal-to-blank ratio (S/B, red lines) with **A)** CAb concentration; **B)** CAb incubation time; **C)** sandwich immunocomplex formation protocol involving sequential biomodifications in (I) three steps, (II-III) two steps, and (IV) one step, (see main text); **D)** TIM-1 incubation time; **E)** b-DAb concentration; **F)** Strep-HRP dilution factor; and **G)** b-DAb/Strep-HRP incubation time. Error bars were estimated as three times the standard deviation of the measurements (n = 3).

for each checked variable, whose tested ranges, and selected values are summarized in Table 1.

The first optimized experimental variable was the CAb concentration (Fig. 2A). The measurements evidenced that in the absence of immobilized CAb, the interactions between the TIM-1 protein, b-DAb, or Strep-HRP conjugate on activated and blocked HOOC-MBs were negligible (see "bars 0.0" in Fig. 2A). This confirmed the efficiency of the ETA-blocking solution to minimize nonspecific adsorptions and, therefore, the feasibility of the sandwich-type immunoassay for determining TIM-1. Fig. 2A shows that the S/B ratio increased significantly with the CAb concentration over the 5.0–100 μg mL^{-1} range and decreased for large CAb concentrations. At 100 μg mL^{-1}, the CAb density on the MBs surface was sufficiently high to maximize the TIM-1 capture probability because the antigen-binding sites were not sterically hindered. However, the slight decrease in the S/B ratio observed for 200 μg mL^{-1} can be explained by CAb saturation on the MBs surface, thus limiting the accessibility of the analyte to antigen-binding sites [51,52]. As a compromise between sensitivity and cost affordability, 50 μg mL^{-1} was selected as the CAb concentration for further experiments. Fig. 2B shows as 15 min were sufficient to enable effective covalent immobilization of CAb. The effect observed for longer incubation times can again be attributed to less efficient target recognition due to steric hindrance when a large amount of CAb molecules was immobilized on the MBs.

Following the CAb's concentration and incubation time optimization, four sandwich immunocomplex formation protocols were tested to balance sensitivity, simplicity, and immunoassay time. Sequential biomodification steps of 30 min each were accomplished by starting from the blocked CAb/MBs.

- **Protocol I** involved three sequential incubation steps with solutions containing (i) 0 or 2500 pg mL^{-1} TIM-1, (ii) 1.0 μg mL^{-1} b-DAb, and (iii) 1/1000 diluted Strep-HRP.
- **Protocol II** involved two sequential incubation steps with solutions containing (i) 0 or 2500 pg mL^{-1} TIM-1 and (ii) 1.0 μg mL^{-1} b-DAb and 1/1000 diluted Strep-HRP mixture.
- **Protocol III** involved two sequential incubation steps with solutions containing (i) 0 or 2500 pg mL^{-1} TIM-1 and 1.0 μg mL^{-1} b-DAb mixture and (ii) 1/1000 diluted Strep-HRP.
- **Protocol IV** involved one incubation step with 0 or 2500 pg mL^{-1} TIM-1, 1.0 μg mL^{-1} b-DAb, and 1/1000 diluted Strep-HRP solution mixture.

According to the results displayed in Fig. 2C, the S/B ratio was notably larger when using protocol II. We hypothesize that the higher effectiveness of this protocol is due to the favored interactions at each modification step. For example, the TIM-1/CAb interaction was favored in the first step as different TIM-1 epitopes remained available to interact with b-DAb. Therefore, incubation with the b-DAb/Strep-HRP mixture solution in the second step might maximize the affinity binding between them without having a steric hindrance effect on the b-DAb/TIM-1 interaction. The other protocols resulted in lower capture and labeling efficiencies, most likely due to aggregation phenomena or steric hindrance when the corresponding bioreagents coexisted in the solution. An incubation time of 15 with the TIM-1 solution provided a larger S/B ratio, while longer times did not improve the sensitivity (Fig. 2D). The effect of the b-DAb concentration (Fig. 2E) and Strep-HRP dilution factor (Fig. 2F) led us to select values of 1.0 μg mL^{-1} and 1/500, respectively. Interestingly, when larger b-DAb and Strep-HRP concentrations were used, notably increased blanks, and decreased specific signals were observed and, consequently, the S/B ratio decreased. According to the hypothesis made for the efficiency of protocol II, the selected concentrations simultaneously promote biorecognition and labeling interaction, limiting the process of agglomeration, steric hindrance, and nonspecific adsorptions. The b-DAb/Strep-HRP incubation process required only 30 min to achieve the best analytical performance, as shown in Fig. 2G.

Therefore, optimization studies suggest that the determination of TIM-1 required only two biomodification steps lasting 45 min, starting from the blocked CAb/MBs conjugates. It is also important to note that these optimization studies, as indicated in the "0.0" bars of panels A and E in Fig. 2, confirmed that the determination of TIM-1 occurred through the formation of sandwich-like immune complexes on the MBs surface.

Table 1
Optimized key experimental variables involved in the amperometric determination of TIM-1 with the developed immunoplatform.

Variable	Tested range	Selected value
[CAb] (μg mL^{-1})	0.0–200.0	50.0
CAb incubation time (min)	5–60	15
Sandwich immunocomplex formation protocol	I–IV	II
TIM-1 incubation time (min)	5–60	15
[b-DAb] (μg mL^{-1})	0.0–5.0	1.0
Strep-HRP dilution factor	1/5000–1/250	1/500
b-DAb/Strep-HRP incubation time (min)	15–60	30

3.2. Analytical performance and remarkable features of the developed immunoplatform

Once the optimal conditions for the amperometric determination of TIM-1 were established, the analytical performance of the immunoplatform was assessed by measuring in different solutions containing known TIM-1 concentrations ranging from 100 to 7500 pg mL^{-1}. Fig. 3A shows that the amperometric response was TIM-1 concentration-dependent. Fig. 3B shows a linear correlation between the amperometric response and TIM-1 concentration over the 87–7500 pg mL^{-1} range fitting equation -i (nA) = (0.448 ± 0.009) [TIM-1, pg mL^{-1}] + (88 ± 29) with a correlation coefficient $r^2 = 0.997$. The limit of detection (LOD = 3 × s_B/slope) and limit of quantification (LOQ = 10 × s_B/slope) were 26 and 87 pg mL^{-1}, respectively, with a standard deviation of the blank (s_B) of 5.5 nA (n = 10).

Unfortunately, to the best of our knowledge, the TIM-1 levels in blood or tumor tissue of patients with breast and lung cancer are not available in the literature. However, a work on TIM-1 levels in the plasma of patients with clear-cell carcinoma set a threshold of 142 pg mL^{-1} [53]. Taking this as the cut-off value, it can be concluded that the LOD provided by the developed immunoplatform allows clinical differentiation between healthy individuals and cancer patients. A relative standard deviation (RSD) value of 3.6% (amperometric responses of 10 different immunoplatforms for a 2500 pg mL^{-1} TIM-1 solution), indicated a high reproducibility.

Table 2 compares the analytical performance and main features of the developed immunoplatform with those of other electrochemical (bio)assays reported so far to determine TIM-1. Considering the analytical performance, the LOD achieved is comparable to some reported values [28,30], not as low as others [26,27,29], but within the range of clinical relevance noted above. It is also important to note that the other electrochemical biosensors described to date require the use of nanomaterials whose preparation and modification imply complex, multi-step protocols that, in many cases, take several days to be completed [28–30] and must be carried out by personnel with a certain degree of specialization.

3.3. Selectivity of the amperometric immunoassay

The selectivity of the immunoplatform was evaluated by testing several interfering non-target proteins that could be present in biological samples. The interfering compounds tested included circulating proteins (IgG, Hb, and HSA) and circulating and tumor tissue biomarkers (TNFα, POSTN, and IL-13Rα2) [54–59]. These potential interfering proteins were checked at the concentrations commonly found in biological samples. The cross-reactivity of each possible interfering non-target protein was studied in the presence (2500 pg mL^{-1}) and in the

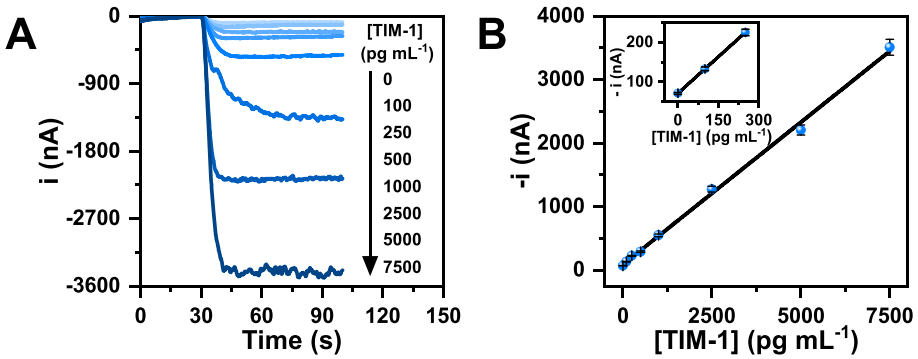

Fig. 3. A) Amperograms recorded with the developed immunoplatform for different TIM-1 concentrations; **B)** calibration curve and linear regression with the data at low concentrations as inset. Error bars were estimated as three times the measurement's standard deviation (n = 3).

Table 2
Comparison of the analytical performance and remarkable features of electrochemical (bio)assays and (bio)sensors reported for the determination of TIM-1.

Detection strategy	Technique	L.R., pg mL^{-1}	LOD, pg mL^{-1}	Assay preparation time[a]/Testing time[b]	Storage stability	Applicability	Ref.
Direct electrochemical detection using HAp-modified CPE	LSV [c] SWV [d]	10000–200000[c] 10000–100000[d]	17000 [c]	Not fully detailed (HAp powders preparation: ~18 h)	Not reported	Spiked urine	[27]
Sandwich-type immunoassay with specific capture antibodies on AuNPs modified GCE, and ABEI-PEI-PFO dots-RGOs/PtNPs nanocomposite-labeled detection antibodies	ECL	0.0500–1000	0.0167	Assay preparation time: ~13 h (+ABEI-PEI-PFO dots-RGOs/Pt NPs@Ab_2-BSA complex: ~18 h)/ Testing time: Not reported	Not reported	Spiked serum	[26]
Sandwich-type immunoassay with specific capture antibodies on $CuCl_2$ NWs with AuNPs modified GCE, and PdPtBP MNPs/ MXene nanocomposite-labeled detection antibodies	DPV	500–100000	86	Assay preparation time: ~2 h (+Ab_2/PdPtBP MNPs/MXene: ~49 h; $CuCl_2$ NWs: ~10 min) Testing time: ~2 h	10 days	Spiked urine	[28]
Sandwich-type immunoassay with specific capture antibodies on COFs-AuNPs modified GCE, and $NiCo_2S_4$@CeO_2 microspheres-labeled detection antibodies	DPV	0.010–50	0.002	Assay preparation time: ~1 h 10 min (+COFs-AuNPs: ~1 h 15 min; Ab_2/$NiCo_2S_4$@CeO_2: ~43 h)/ Testing time: ~ 15 min	7 weeks	Spiked plasma	[29]
Label-free immunoassay with specific capture antibodies on Au-Galinstan Nds modified paper-based disposable electrode	EIS	100–1000000	64	Assay preparation time: >1 h (+Au-Galinstan Nds: ~72 h)/Testing time: Not reported	20 days	Spiked serum	[30]
Magnetic sandwich-type immunoassay with capture antibodies conjugated-magnetic beads, and Strep-HRP-labeled detection antibodies	Amperometry	87–7500	26	Assay preparation time: 2.2 h/ Testing time: 45 min	22 days	Cancer cultured cell extracts	This work

Abbreviations: ABEI-PEI-PFO dots-RGOs/PtNPs: Pt nanoparticles (PtNPs) supported on reduced graphene oxide nanosheets (RGOs) as the loading platform of N-(aminobutyl)-N-(ethylisoluminol)-polyethylenimine-poly(9,9-dioctylfluorenyl-2,7-diyl) (ABEI-PEI-PFO) dots; AuNPs: gold nanoparticles; COFs-AuNPs: gold nanoparticles-modified covalent organic frameworks (COFs); CPE: carbon paste electrode; $CuCl_2$ NWs: copper chloride nanowires; DPV: differential pulse voltammetry; ECL: electrochemiluminescence; EIS: electrochemical impedance spectroscopy; Galinstan: 68.5% gallium (Ga), 21.5% indium (In), and 10% tin (Sn); GCE: glassy carbon electrode; HAp: hydroxyapatite; LSV: linear sweep voltammetry; Nds: nanodendrites; $NiCo_2S_4$@CeO_2: cerium oxide (CeO_2) nanosheet-coated nickel/cobalt bimetallic sulfides ($NiCo_2S_4$) microspheres; PdPtBP MNPs: quaternary metallic/nonmetallic palladium/platinum/boron/phosphorus (PdPtBP) alloy on mesoporous nanoparticles (MNPs)-based nanozymes; Strep-HRP: streptavidin-horseradish peroxidase conjugate; SWV: square wave voltammetry.

[a] Estimated time to prepare immunosensor and nanomaterials included before application of the sample to system.

[b] Estimated time from applying the sample to the system until signal measurement.

[c] Linear range and LOD determined in model buffer solution by LSV.

[d] Linear range determined in spiked human urine by SWV.

absence of TIM-1. The results shown in Fig. 4 indicated that the amperometric response for 2500 pg mL^{-1} TIM-1 was remarkably larger than those measured for the blank and for each of the interfering non-target proteins individually tested. In addition, the amperometric response showed statistically significant differences with a level of statistical significance of 95%, indicating high specificity.

Furthermore, statistically significant differences in the amperometric response for 2500 pg mL^{-1} TIM-1 were observed in the presence of IgG and HSA at the same level of statistical significance, indicating that IgG and HSA exhibited a slight cross-reactivity. IgG can recognize the light chains and Fc regions of the CAb and those of the b-DAb, thus enhancing the amperometric response and explaining the observed response [60, 61]. On the other hand, HSA can prevent interaction between TIM-1 and CAb due to steric hindrance, thus decreasing the amperometric response. The slight interference from these two non-target proteins, which would only be an issue for the analysis of blood samples, might be minimized after a simple sample dilution. None of the other tested non-target proteins exhibited significant cross-reactivity, indicating high selectivity. In addition, it is worth mentioning that according to specificity studies conducted by the supplier company, the bioreagents used in the immunoassay did not exhibit any cross-reactivity against 50 ng mL^{-1} of recombinant human TIM-3/Fc chimera and TIM-4 proteins.

3.4. *Stabilitity of the immunoconjugates*

CAb/MBs conjugates can be provided to the end user as a "stock reagent" for POCT solutions, which will speed up the whole analysis time by simplifying the entire protocol. Therefore, the long-term storage

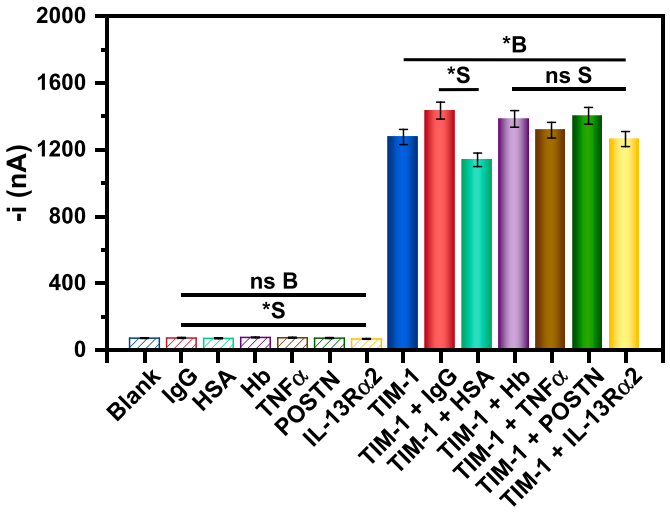

Fig. 4. Comparison of the amperometric responses obtained with the developed immunoplatform for 1 mg mL^{-1} IgG, 50 mg mL^{-1} HSA, 2.5 mg mL^{-1} Hb, 5 ng mL^{-1} TNFα, 5 ng mL^{-1} POSTN, and 50 ng mL^{-1} IL-13Rα2 in the presence of 2500 pg mL^{-1} (filled bars) and the absence (pattern bars) of TIM-1 standard protein. ***B** indicates statistically significant differences concerning the blank (0 pg mL^{-1} TIM-1, *p*-value <0.05), and **ns B** indicates non-statistically significant differences concerning the blank (0 pg mL^{-1} TIM-1, *p*-value >0.05). ***S** indicates statistically significant differences concerning the signal (2500 pg mL^{-1} of TIM-1, *p*-value <0.05), and **ns B** indicates non-statistically significant differences concerning the signal (2500 pg mL^{-1} of TIM-1, *p*-value >0.05). Error bars were estimated as three times the measurement's standard deviation (n = 3).

stability of the CAb/MBs conjugates was checked by resuspending them in 50 μL of filtered 1X PBS pH 7.5 and storage at 4 °C. Fig. 5 shows the amperometric responses measured in the presence and in the absence of 2500 pg mL^{-1} of TIM-1 standard protein with different immunoplatforms prepared from the stored CAb/MBs conjugates. The constructed control chart shows as the S/B ratio remained within the control limits for twenty-two days, suggesting that CAb/MBs conjugates could be

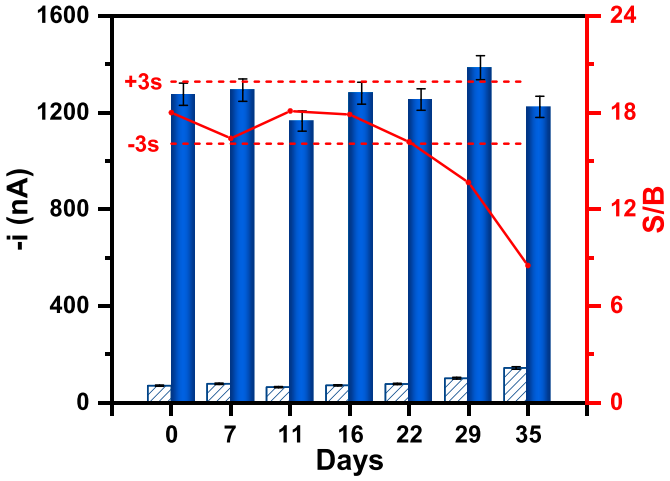

Fig. 5. Long-term stability studies of the CAb/MBs conjugates stored at 4 °C in filtered 1X PBS pH 7.5. Amperometric responses provided by immunoplatforms prepared from the stored CAb/MBs in the presence (blue bars) and in the absence (white pattern bars) of 2500 pg mL^{-1} TIM-1 standard protein, and the resulting signal-to-blank ratio (S/B, red lines). Control limits (red dashed lines) were set as three times the standard deviation of the signal-to-blank mean value ($\bar{x}_{S/B} \pm 3s_{S/B}$) of three measurements obtained on the first day of CAb/MBs conjugates preparation. Error bars were estimated as three times the measurement's standard deviation (n = 3).

prepared and stored for three weeks until their use.

3.5. Analysis of cancer cultured cell extracts

The developed bioplatform was applied to the determination of TIM-1 in extracts of breast (MDA-MB-231, MCF7, and SkBr3) and lung (A549) cancer cells. For this purpose, the amount of extract to be used for the analysis and the possible presence of matrix effect were evaluated. An extract amount of 0.25 μg was sufficient for the analysis of the samples (results not shown). On the other hand, a matrix effect was found for most extracts as indicated by the statistical comparison of the slope value for the calibration curve of TIM-1 standards prepared in the buffer solution and the values for the calibrations constructed in the presence of 0.25 μg of each of the extracts (Table 3). Accordingly, the standard additions method was employed to carry out the determinations.

The concentration of TIM-1 provided by the bioplatform in each of the cell extracts are shown in Fig. 6 and summarized in Table 4.

Quantitative and semiquantitative results obtained with the bioplatform and WB analysis, respectively, were in pretty good agreement and confirmed the expression of TIM-1 in the 4 cell protein extracts analyzed, similar in MCF7 and SkBr3 cells and much higher in MDA-MB-231 cells. These results agree with data obtained from the Human Protein Atlas database [62], which states high-intensity staining with polyclonal antibodies selective to TIM-1 of tumor cells in breast cancer (MDA-MB-231) and moderate in non-small cell lung cancer, NSCLC (A549) [63]. Indeed, studies carried out by Zheng et al. revealed that depletion of TIM-1 could significantly inhibit cell viability as well as the migration and invasion abilities of A549 cells [14].

It is important to note that the electrochemical (bio)sensors reported to date for the determination of TIM-1 were only applied to spiked biofluids (serum, plasma, and urine) [26–30]. Moreover, the results given in this work are the first quantitative results for TIM-1 expression in this type of cell extracts and, according to that reported by Zheng et al. [14], they can be related to the potential of cells to migrate and invade.

4. Conclusions

A disposable sandwich immunoplatform assisted by using MBs was developed for the selective, and rapid amperometric determination of TIM-1 at SPCE using HQ/H_2O_2/HRP redox system. The immunoplatfom exhibited excellent analytical performance, with a LOD value of 26 pg mL^{-1} of TIM-1 standards in buffered solutions. The developed immunoplatform is competitive with other reported electrochemical biosensing strategies in terms of simplicity and assay time. Moreover, the employed amperometric transduction is the most widely implemented electrochemical detection technique to date in point-of-need devices, such as a glucometer. All these features make the developed immunoplatform ideal for future implementation in this type of devices. In addition, the immunoplatform has successfully tackled the analysis of breast and lung cancer cell extracts, providing the first quantitative results for such samples, which, according to recent research, may be used to discriminate the potential of cells to migrate and invade.

Table 3
Comparison between the slope values (in nA pg^{-1} mL) of the calibration plots constructed with the developed immunoplatform for TIM-1 standards prepared in buffer solution and in the presence of 0.25 μg of each of the analyzed extracts.

Medium	Slope, nA pg^{-1} mL	t_{exp}[a]	t_{tab} (α = 0.05)
Buffered solution	0.448 ± 0.009	–	–
MDA-MB-231	0.37 ± 0.01	2.677	$t_{tab\ (0.05;9)}$ = 2.262
MCF7	0.37 ± 0.02	3.056	
SkBr3	0.374 ± 0.006	2.948	
A549	0.487 ± 0.006	1.508	

[a] t_{exp} estimated by comparing the slope value obtained for standards prepared in the corresponding extract and in buffered solutions.

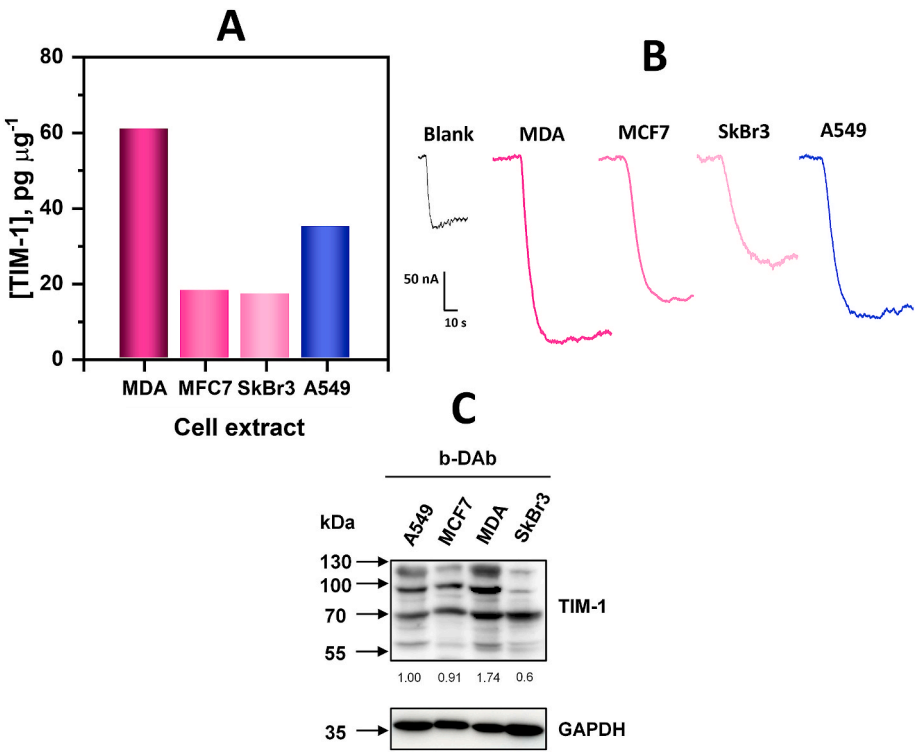

Fig. 6. A) Concentrations of TIM-1 determined with the developed immunoplatform in the tested cell extracts. **B**) Amperometric responses recorded with the immunoplatform for 0.25 µg of each extract. **C)** WB analysis of the same cell extracts (10.0 µg of each cell lysate were blotted to nitrocellulose membranes and probed with b-DAb). Protein bands were quantified by densitometry. GAPDH was used as loading control and for normalization purposes.

Table 4
TIM-1 concentrations ($\bar{x} \pm ts/\sqrt{n}$; n = 3; α = 0.05) determined with the immunoplatform in each cell extract analyzed.

Extract	[TIM-1] pg μg^{-1}	RSD, %
A549	35 ± 2	2.0
MDA-MB-231	61 ± 4	2.2
MCF7	18 ± 4	7.3
SkBr3	17 ± 2	2.9

Credit author statement

Jennifer Quinchia: Methodology, Investigation, Writing, Review & editing-original draft. **Marina Blázquez-García:** Methodology, Investigation, Review & editing-original draft. **Rebeca M. Torrente-Rodríguez:** Supervision, Review & editing-original draft. **Víctor Ruiz-Valdepeñas Montiel:** Supervision, Review & editing-original draft. **Verónica Serafín:** Supervision, Review & editing-original draft. **Raquel Rejas-González:** Investigation, Review & editing-original draft. **Ana Montero-Calle:** Investigation, Review & editing-original draft. **Jahir Orozco:** Resources, Writing, Review & editing-original draft, Funding acquisition. **José M. Pingarrón:** Resources, Review & editing original draft. **Rodrigo Barderas:** Supervision, Resources, Writing, Review & editing-original draft, Funding acquisition. **Susana Campuzano:** Conceptualization, Supervision, Resources, Writing, Review & editing original draft, Funding acquisition.

Declaration of competing interest

The authors declare that they have no known competing financial interests or personal relationships that could have appeared to influence the work reported in this paper.

Data availability

Data will be made available on request.

Acknowledgements

The financial support of PID2019-103899RB-I00 (Spanish Ministerio de Ciencia e Innovación) Research Projects and PI20CIII/00019 Grant from the AES-ISCIII Program co-founded by FEDER funds and the TRANSNANOAVANSENS-CM Program from the Comunidad de Madrid (Grant S2018/NMT-4349) are gratefully acknowledged. A.M-C. was supported by a FPU predoctoral contract supported by the Spanish Ministerio de Educación, Cultura y Deporte. J.Q. was founded by Minciencias, Mineducacion, MINCIT, and ICETEX through the Program Ecosistema Cientifico Cod. FP44842-211–2018, project number 58536. J.O. thanks support from the University of Antioquia and the Max Planck Society through the cooperation agreement 566–1, 2014.

References

[1] N. Wichukchinda, T. Nakajima, N. Saipradit, E.E. Nakayama, H. Ohtani, A. Rojanawiwat, P. Pathipvanich, K. Ariyoshi, P. Sawanpanyalert, T. Shioda, A. Kimura, TIM1 haplotype may control the disease progression to AIDS in a HIV-1-infected female cohort in Thailand, AIDS 24 (11) (2010) 1625–1631, https://doi.org/10.1097/QAD.0b013e32833a8e6d.
[2] P. Du, R. Xiong, X. Li, J. Jiang, Immune regulation and antitumor effect of TIM-1, J. Immunol. Res. 2016 (2016), 8605134, https://doi.org/10.1155/2016/8605134.
[3] W.K. Han, V. Bailly, R. Abichandani, R. Thadhani, J.V. Bonventre, Kidney Injury Molecule-1 (KIM-1): a novel biomarker for human renal proximal tubule injury, Kidney Int. 62 (1) (2002) 237–244, https://doi.org/10.1046/j.1523-1755.2002.00433.x.
[4] J.V. Bonventre, Kidney Injury Molecule-1 (KIM-1): a specific and sensitive biomarker of kidney injury, Scand. J. Clin. Lab. Invest. 68 (S241) (2008) 78–83, https://doi.org/10.1080/00365510802145059.
[5] J.V. Bonventre, Kidney Injury Molecule-1 (KIM-1): a urinary biomarker and much more, Nephrol. Dial. Transplant. 24 (11) (2009) 3265–3268, https://doi.org/10.1093/ndt/gfp010.

[6] J.J. McIntire, D.T. Umetsu, R.H. DeKruyff, TIM-1, a novel allergy and asthma susceptibility gene, Springer Semin. Immunopathol. 25 (3–4) (2004) 335–348, https://doi.org/10.1007/s00281-003-0141-3.

[7] D.T. Umetsu, S.E. Umetsu, G.J. Freeman, R.H. DeKruyff, TIM gene family and their role in atopic disease, Curr. Top. Microbiol. Immunol. 321 (2008) 201–215, https://doi.org/10.1007/978-3-540-75203-5_10.

[8] R. Rodriguez-Manzanet, R. Dekruyff, V.K. Kuchroo, D.T. Umetsu, The costimulatory role of TIM molecules, Immunol. Rev. 229 (1) (2009) 259–270, https://doi.org/10.1111/j.1600-065X.2009.00772.x.

[9] H.Y. Kim, M.B. Eyheramonho, M. Pichavant, C.G. Cambaceres, P. Matangkasombut, G. Cervio, S. Kuperman, R. Moreiro, K. Konduru, M. Manangeeswaran, G.J. Freeman, A polymorphism in TIM1 is associated with susceptibility to severe hepatitis A virus infection in humans, J. Clin. Invest. 121 (3) (2011) 1111–1118, https://doi.org/10.1172/JCI44182.

[10] S. Hu, Y. Xie, N. Zhou, L. Jin, Y. Tan, D. Liu, Y. Gong, L. Liu, J. Liu, W. Liu, Y. Chen, Expression of T-cell immunoglobulin-and mucin-domain-containing molecules-1 and-3 (Tim-1 and Tim-3) in Helicobacter Pylori infection, Helicobacter 16 (5) (2011) 373–381, https://doi.org/10.1111/j.1523-5378.2011.00855.x.

[11] T.L. Mosbruger, P. Duggal, J.J. Goedert, G.D. Kirk, W.K. Hoots, L.H. Tobler, M. Busch, M.G. Peters, H.R. Rosen, D.L. Thomas, C. Thio, Large-scale candidate gene analysis of spontaneous clearance of Hepatitis C virus, J. Infect. Dis. 201 (9) (2010) 1371–1380, https://doi.org/10.1086/651606.

[12] Y. Wang, T.A. Martin, W.G. Jiang, HAVcR-1 expression in human colorectal cancer and its effects on colorectal cancer cells in vitro, Anticancer Res. 33 (1) (2013) 207–214.

[13] E.J.A. Telford, W.G. Jiang, T.A. Martin, HAVcR-1 involvement in cancer progression, Histol. Histopathol. 32 (2) (2017) 121–128, https://doi.org/10.14670/HH-11-817.

[14] X. Zheng, K. Xu, L. Chen, Y. Zhou, J. Jiang, Prognostic value of TIM-1 expression in human non-small-cell lung cancer, J. Transl. Med. 17 (2019) 178, https://doi.org/10.1186/s12967-019-1931-2.

[15] X. Kong, M. Fu, X. Niu, H. Jiang, Comprehensive analysis of the expression, relationship to immune infiltration and prognosis of TIM-1 in cancer, Front. Oncol. 10 (2020) 1–11, https://doi.org/10.3389/fonc.2020.01086, 1986.

[16] L. Chen, J. Qing, Y. Xiao, X. Huang, Y. Chi, Z. Chen, TIM-1 promotes proliferation and metastasis, and inhibits apoptosis, in cervical cancer through the PI3K/AKT/P53 pathway, BMC Cancer 22 (1) (2022) 1–17, https://doi.org/10.1186/s12885-022-09386-7.

[17] T.A. Martin, G.M. Harrison, M.D. Mason, W.G. Jiang, HAVcR-1 reduces the integrity of human endothelial tight junctions, Anticancer Res. 31 (2) (2011) 467–473.

[18] G. Diniz, A.G. Pulular, D.S. Kahraman, U. Varol, S. Sayhan, D. Ayaz, C. Karaali, Tissue expression of neutrophil gelatinase-associated lipocalin and Kidney Injury Molecule-1 in breast cancers, Eur J Breast Health 18 (2022) 336–342, https://doi.org/10.4274/ejbh.galenos.2022.2022-5-1.

[19] V.S. Vaidya, G.M. Ford, S.S. Waikar, Y. Wang, M.B. Clement, V. Ramirez, W. E. Glaab, S.P. Troth, F.D. Sistare, W.C. Prozialeck, J.R. Edwards, N.A. Bobadilla, S. C. Mefferd, J.V. Bonventre, A rapid urine test for early detection of kidney injury, Kidney Int. 76 (1) (2009) 108–114, https://doi.org/10.1038/ki.2009.96.

[20] S.H. Lee, H.S. Lee, G. Park, S.M. Oh, D.S. Oh, Dual actions on gout flare and acute kidney injury along with enhanced renal transporter activities by Yokuininto, a Kampo Medicine, BMC Compl. Alternative Med. 19 (2019) 57, https://doi.org/10.1186/s12906-019-2469-9.

[21] V.S. Vaidya, S.S. Waikar, M.A. Ferguson, F.B. Collings, K. Sunderland, C. Gioules, G. Bradwin, R. Matsouaka, R.A. Betensky, G.C. Curhan, J.V. Bonventre, Urinary biomarkers for sensitive and specific detection of acute kidney injury in humans, Clin. Transl. Sci. 1 (3) (2008) 200–208, https://doi.org/10.1111/j.1752-8062.2008.00053.x.

[22] H.J. Chung, K.L. Pellegrini, J. Chung, K. Wanigasuriya, I. Jayawardene, K. Lee, H. Lee, V.S. Vaidya, R. Weissleder, Nanoparticle detection of urinary markers for point-of-care diagnosis of kidney injury, PLoS One 10 (7) (2015), e0133417, https://doi.org/10.1371/journal.pone.0133417.

[23] E. Zeidan, S. Li, Z. Zhou, J. Miller, M.G. Sandros, Single-multiplex detection of organ injury biomarkers using SPRi based nano-immunosensor, Sci. Rep. 6 (2016) 2–9, https://doi.org/10.1038/srep36348.

[24] J. Luan, T. Xu, J. Cashin, J.J. Morrissey, E.D. Kharasch, S. Singamaneni, Environmental stability of plasmonic biosensors based on natural versus artificial antibody, Anal. Chem. 90 (13) (2018) 7880–7887, https://doi.org/10.1021/acs.analchem.7b05470.

[25] J. Luan, J.J. Morrissey, Z. Wang, H.G. Derami, K.K. Liu, S. Cao, Q. Jiang, C. Wang, E.D. Kharasch, R.R. Naik, S. Singamaneni, Add-on plasmonic patch as a universal fluorescence enhancer, Light Sci. Appl. 7 (1) (2018) 29, https://doi.org/10.1038/s41377-018-0027-8.

[26] H. Yang, H. Wang, C. Xiong, Y. Chai, R. Yuan, Highly sensitive electrochemiluminescence immunosensor based on ABEI/H_2O_2 system with PFO dots as enhancer for detection of Kidney Injury Molecule-1, Biosens. Bioelectron. 116 (2018) 16–22, https://doi.org/10.1016/j.bios.2018.05.032.

[27] Y. Zhang, W. Zhang, Q. Zhang, K. Li, W. Liu, Y. Liu, C.E. Banks, Green electrochemical sensing platforms: utilizing hydroxyapatite derived from natural fish scales as a novel electrochemical material for the sensitive detection of Kidney Injury Molecule 1 (KIM-1), Analyst 139 (21) (2014) 5362–5366, https://doi.org/10.1039/c4an00957f.

[28] C. Liu, W. Yang, X. Min, D. Zhang, X. Fu, S. Ding, W. Xu, An enzyme-free electrochemical immunosensor based on quaternary metallic/nonmetallic PdPtBP alloy mesoporous nanoparticles/MXene and conductive $CuCl_2$ nanowires for ultrasensitive assay of Kidney Injury Molecule-1, Sensors Actuators, B Chem. 334 (2021), 129585, https://doi.org/10.1016/j.snb.2021.129585.

[29] H. Boyacıoğlu, B.B. Yola, C. Karaman, O. Karaman, N. Atar, M.L. Yola, A novel electrochemical kidney injury molecule-1 (KIM-1) immunosensor based covalent organic frameworks-gold nanoparticles composite and porous $NiCo_2S_4$@CeO_2 microspheres: the monitoring of acute kidney injury, Appl. Surf. Sci. 578 (2022), 152093, https://doi.org/10.1016/j.apsusc.2021.152093.

[30] M. Das, T. Chakraborty, C. Yu Lin, K. Fong Lei, C. Haur Kao, Hierarchical gold-galinstan nanodendrites modified disposable immunosensor for the label-free detection of KIM-1 by antibody immobilization on Staphylococcal Protein A, Appl. Surf. Sci. 607 (2023), 154930, https://doi.org/10.1016/j.apsusc.2022.15493.

[31] U. Anik, Electrochemical medical biosensors for POC applications, in: In Medical Biosensors for Point of Care (POC) Applications, Woodhead Publishing, 2017, pp. 275–292, https://doi.org/10.1016/B978-0-08-100072-4.00012-5.

[32] J. Quinchia, D. Echeverri, A.F. Cruz-Pacheco, M.E. Maldonado, J.A. Orozco, Electrochemical biosensors for determination of colorectal tumor biomarkers, Micromachines 11 (4) (2020) 1–46, https://doi.org/10.3390/MI11040411.

[33] A.M. Kumar, K. Kachhawa, Biomedical applications of bioelectrochemical sensors, in: Multifaceted Bio-Sensing Technology, Academic Press, 2023, pp. 239–260, 4.

[34] A. Khanmohammadi, A. Aghaie, E. Vahedi, A. Qazvini, A.A. Ghanei, A. Hajian, H. Bagheri, Electrochemical biosensors for the detection of lung cancer biomarkers: a review, Talanta 206 (2020), 120251, https://doi.org/10.1016/j.talanta.2019.120251.

[35] M.R. Hasan, M.S. Ahommed, M. Daizy, M.S. Bacchu, M.R. Ali, M.R. Al-Mamun, M. Aly Saad Aly, M.Z.H. Khan, S.I. Hossain, Recent development in electrochemical biosensors for cancer biomarkers detection, Biosens. Bioelectron-X 8 (2021), 100076, https://doi.org/10.1016/j.biosx.2021.100075.

[36] S.I. Kaya, G. Ozcelikay, F. Mollarasouli, N.K. Bakirhan, S.A. Ozkan, Recent achievements and challenges on nanomaterial based electrochemical biosensors for the detection of colon and lung cancer biomarkers, Sensor. Actuator. B Chem. 351 (15) (2022), 130856, https://doi.org/10.1016/j.snb.2021.130856.

[37] C. Zhu, G. Yang, H. Li, D. Du, Y. Lind, Electrochemical sensors and biosensors based on nanomaterials and nanostructures, Anal. Chem. 87 (2015) 230–249, https://doi.org/10.1007/s12598-017-0955-0.

[38] C. Dincer, R. Bruch, E. Costa-Rama, M.T. Fernández-Abedul, A. Merkoçi, A. Manz, G.A. Urban, F. Güder, Disposable sensors in diagnostics, food, and environmental monitoring, Adv. Mater. 31 (30) (2019), 1806739, https://doi.org/10.1002/adma.201806739.

[39] N. Wongkaew, M. Simsek, C. Griesche, A.J. Baeumner, Functional nanomaterials and nanostructures enhancing electrochemical biosensors and lab-on-a-chip performances: recent progress, applications, and future perspective, Chem. Rev. 119 (1) (2019) 120–194, https://doi.org/10.1021/acs.chemrev.8b00172.

[40] M.E. Cortina, L.J. Melli, M. Roberti, M. Mass, G. Longinotti, S. Tropea, P. Lloret, D. A. Rey Serantes, F. Salomón, M. Lloret, A.J. Caillava, S. Restuccia, J. Altcheh, C. A. Buscaglia, L. Malatto, J.E. Ugalde, L. Fraigi, C. Moina, G. Ybarra, A.E. Ciocchini, D.J. Comerci, Electrochemical magnetic microbeads-based biosensor for point-of-care serodiagnosis of infectious diseases, Biosens. Bioelectron. 80 (2016) 24–33, https://doi.org/10.1016/j.bios.2016.01.021.

[41] J. Kudr, B. Klejdus, V. Adam, O. Zitka, Magnetic solids in electrochemical analysis, TrAC-Trends Anal. Chem. 98 (2018) 104–113, https://doi.org/10.1016/j.trac.2017.10.023.

[42] M. Pastucha, Z. Farka, K. Lacina, Z. Mikušová, P. Skládal, Magnetic nanoparticles for smart electrochemical immunoassays: a review on recent developments, Microchim. Acta 186 (2019) 312, https://doi.org/10.1007/s00604-019-3410-0.

[43] F. Mollarasouli, E. Zor, G. Ozcelikay, S.A. Ozkan, Magnetic nanoparticles in developing electrochemical sensors for pharmaceutical and biomedical applications, Talanta 226 (2021) 226, https://doi.org/10.1016/j.talanta.2021.122108.

[44] C. Muñoz-San Martín, A. Montero-Calle, M. Garranzo-Asensio, M. Gamella, V. Perez-Gines, M. Pedrero, J.M. Pingarrón, R. Barderas, N. de los Santos Alvarez, M.J. Lobo-Castañón, S. Campuzano, First bioelectronic immunoplatform for quantitative secretomic analysis of total and metastasis-driven glycosylated haptoglobin, Anal. Bioanal. Chem. 415 (2023) 2045–2057, https://doi.org/10.1007/s00216-022-04397-6.

[45] J.R. Wisniewski, F.Z. Gaugaz, Fast and sensitive total protein and peptide assays for proteomic analysis, Anal. Chem. 87 (2015) 4110–4166, https://doi.org/10.1021/ac504689z.

[46] A. Montero-Calle, M. Garranzo-Asensio, R.M. Torrente-Rodríguez, V. Ruiz-Valdepeñas Montiel, C. Poves, J. Dziaková, R. Sanz, C. Díaz del Arco, J. M. Pingarrón, M.J. Fernández-Aceñero, S. Campuzano, R. Barderas, p53 and p63 p53 and p63 proteoforms derived from alternative splicing possess differential seroreactivity in colorectal cancer with distinct diagnostic ability from the canonical proteins, Cancers 15 (7) (2023) 2102, https://doi.org/10.3390/cancers15072102.

[47] C. Camacho, J.C. Matías, B. Chico, R. Cao, L. Gómez, B.K. Simpson, R. Villalonga, Amperometric biosensor for hydrogen peroxide, using supramolecularly immobilized horseradish peroxidase on the β-cyclodextrin-coated gold electrode, Electroanalysis 19 (24) (2007) 2538–2542, https://doi.org/10.1002/elan.200703993.

[48] S.H. Wu, X.B. Huang, Y. Tang, L.M. Ma, Y. Liu, J.-J. Sun, Temperature controllable electrochemical sensors based on horseradish peroxidase as electrocatalyst at heated Au disk electrode and its preliminary application for H_2O_2 detection, Anal. Chim. Acta 1096 (2020) 44–52, https://doi.org/10.1016/j.aca.2019.10.052.

[49] M. Gamella, S. Campuzano, F. Conzuelo, A.J. Reviejo, J.M. Pingarrón, Amperometric magnetoimmunosensors for direct determination of D-dimer in

human serum, Electroanalysis 24 (12) (2012) 2235–2243, https://doi.org/10.1002/elan.201200503.
[50] B. Esteban-Fernández de Ávila, V. Escamilla-Gómez, S. Campuzano, M. Pedrero, J. M. Pingarrón, Disposable amperometric magnetoimmunosensor for the sensitive detection of the cardiac biomarker amino-terminal pro-B-type natriuretic peptide in human serum, Anal. Chim. Acta 784 (2013) 18–24, https://doi.org/10.1016/j.aca.2013.04.039.
[51] V. Pérez-Ginés, R.M. Torrente-Rodríguez, A. Montero-Calle, G. Solís-Fernández, P. Atance-Gómez, M. Pedrero, J.M. Pingarrón, R. Barderas, S. Campuzano, Tackling CD147 exosome-based cell-cell signaling by electrochemical biosensing for early colorectal cancer detection, Biosens. Bioelectron. X 11 (2022), 100192, https://doi.org/10.1016/j.biosx.2022.100192.
[52] C. Muñoz-San Martín, V. Pérez-Ginés, R.M. Torrente-Rodríguez, M. Gamella, G. Solís-Fernández, A. Montero-Calle, M. Pedrero, V. Serafín, N. Martínez-Bosch, P. Navarro, P. García de Frutos, M. Batlle, R. Barderas, J.M. Pingarrón, S. Campuzano, Electrochemical immunosensing of growth arrest-specific 6 in human plasma and tumor cell secretomes, Electrochem. Sci. Adv. 2 (4) (2022) 1–12, https://doi.org/10.1002/elsa.202100096.
[53] N.E. Kushlinskii, E.S. Gershtein, D.S. Naberezhnov, M.A. Taipov, S.D. Bezhanova, D.Y. Pushkar, V.B. Matveev, I.S. Stilidi, Kidney Injury Molecule-1 (KIM-1) in blood plasma of patients with clear-cell carcinoma, Bull. Exp. Biol. Med. 167 (3) (2019) 388–392, https://doi.org/10.1007/s10517-019-04533-w.
[54] Q.-W. Ben, Z. Zhao, S.-F. Ge, J. Zhou, F. Yuan, Y.-Z. Yaun, Circulating levels of periostin may help identify patients with more aggressive colorectal cancer, Int. J. Oncol. 34 (2009) 821–828, https://doi.org/10.3892/ijo_00000208.
[55] R. Barderas, R.A. Bartolomé, M.J. Fernandez-Aceñero, S. Torres, J.I. Casal, High expression of IL-13 receptor A2 in colorectal cancer is associated with invasion, liver metastasis, and poor prognosis, Cancer Res. 72 (11) (2012) 2780–2790, https://doi.org/10.1158/0008-5472.CAN-11-4090.
[56] O.A. Al Obeed, K.A. Alkhayal, A. Al Sheikh, A.M. Zubaidi, M.A. Vaali-Mohammed, R. Boushey, J.H. Mckerrow, M.H. Abdulla, Increased expression of tumor necrosis factor-α is associated with advanced colorectal cancer stages, World J. Gastroenterol. 20 (48) (2014) 18390–18396, https://doi.org/10.3748/wjg.v20.i48.18390.
[57] Z. Li, X. Zhang, Y. Yang, S. Yang, Z. Dong, L. Du, L. Wang, C. Wang, Periostin expression and its prognostic value for colorectal cancer, Int. J. Mol. Sci. 16 (6) (2015) 12108–12118, https://doi.org/10.3390/ijms160612108.
[58] X. Deng, S. Ao, J. Hou, Z. Li, Y. Lei, G. Lyu, Prognostic significance of periostin in colorectal cancer, Chinese J. Cancer Res. 31 (3) (2019) 547–556, https://doi.org/10.21147/j.issn.1000-9604.2019.03.16.
[59] F. Warsinggih, I. Limanu, R. Labeda, E. Lusikooy Mappincara, M. Faruk, The relationship of tumor necrosis factor alpha levels in plasma toward the stage and differentiation degree in colorectal cancer, Med. Clin. Pract. 4 (2021) 10–13, https://doi.org/10.1016/j.mcpsp.2021.100224.
[60] S.E.F. Melanson, M.J. Tanasijevic, P. Jarolim, Cardiac troponin assays: a view from the clinical chemistry laboratory, Circulation 116 (2007), e501−e504, https://doi.org/10.1161/CIRCULATIONAHA.107.722975.
[61] D. Echeverri, J. Orozco, β-1,4-Galactosyltransferase-V colorectal cancer biomarker immunosensor with label-free electrochemical detection, Talanta 243 (2022), 123337, https://doi.org/10.1016/j.talanta.2022.123337.
[62] The Human Protein Atlas. HAVCR1. URL: https://www. proteinatlas.org/ensg00000113249-havcr1.
[63] T.A. Karmakova, N.S. Sergeeva, K.Yu Kanukoev, B.Ya Alekseev, Kaprin A.D, Kidney injury molecule 1 (KIM-1): a multifunctional glycoprotein and biological marker, Sovrem. Tekhnol. Med. 13 (3) (2021) 64–78, https://doi.org/10.17691/stm2021.13.3.08 (Review).